Supplementary Information for “*scConfluence : single-cell diagonal integration with regularized Inverse Optimal Transport on weakly connected features*”

The Supplementary Information is organized as follows:

- Page 2 of this PDF: Supplementary Note 1
- Pages 3 to 5: Supplementary Tables 1 to 6
- Pages 6 to 13: Supplementary Figures 1 to 18

Supplementary Note 1

The proof only uses two classical results in OT theory. Firstly, there is a primal-dual relationship linking the optimal plan $\mathbf{Q}_\varepsilon(\mathbf{a},\mathbf{b})$ to an optimal pair of potentials $(\mathbf{f},\mathbf{g})$ such that:

$$\mathbf{Q}(\mathbf{a},\mathbf{b}) = \exp(\frac{1}{\varepsilon}(\mathbf{f}\oplus\mathbf{g}-\mathbf{c}_{L_2}(\mathbf{a},\mathbf{b}))$$

Secondly, the optimal value of the entropic OT problem can be expressed with this optimal pair of potentials:

$$(\frac{1}{n_1}\mathbf{1})^T\mathbf{f} + (\frac{1}{n_2}\mathbf{1})^T\mathbf{g} - \varepsilon = OT_\varepsilon^{+\infty}(\mathbf{a},\mathbf{b},c_{L_2})$$

$$\begin{aligned}KL(\mathbf{P}|\mathbf{Q}_\varepsilon(\mathbf{a},\mathbf{b})) &= \langle\mathbf{P},\log(\frac{\mathbf{P}}{\mathbf{Q}_\varepsilon(\mathbf{a},\mathbf{b})})\rangle\\ &= \langle\mathbf{P},\log(\mathbf{P})\rangle - \langle\mathbf{P},\log(\mathbf{Q}_\varepsilon(\mathbf{a},\mathbf{b}))\rangle\\ &= \langle\mathbf{P},\log(\mathbf{P})\rangle - \langle\mathbf{P},\frac{1}{\varepsilon}(\mathbf{f}\oplus\mathbf{g}-\mathbf{c}_{L_2}(\mathbf{a},\mathbf{b}))\rangle\\ &= \langle\mathbf{P},\log(\mathbf{P})\rangle + \frac{1}{\varepsilon}\langle\mathbf{P},\mathbf{c}_{L_2}(\mathbf{a},\mathbf{b}))\rangle - \frac{1}{\varepsilon}\langle\mathbf{P},\mathbf{f}\oplus\mathbf{g}\rangle\end{aligned}$$

$$\begin{aligned}\langle\mathbf{P},\mathbf{f}\oplus\mathbf{g}\rangle &= (\mathbf{P}\mathbf{1})^T\mathbf{f} + (\mathbf{P}^T\mathbf{1})^T\mathbf{g}\\ &= (\frac{1}{n_1}\mathbf{1})^T\mathbf{f} + (\frac{1}{n_2}\mathbf{1})^T\mathbf{g}\\ &= OT_\varepsilon^{+\infty}(\mathbf{a},\mathbf{b},c_{L_2}) + \varepsilon\end{aligned}$$

Supplementary Table 1. List of the datasets used in this paper and their characteristics.

Dataset Name	**Technology**	**Modalities**	**Organism**	**Tissue**	**Cells (after QC)**	**Labels**	**Batches**	**Reference**
Cell lines	scCAT-seq	RNA, ATAC	Human	Cell lines	206	3	1	Liu, L. et al[1]
PBMC 10X	10X Multiome	RNA, ATAC	Human	PBMC	9,378	14	1	10X genomics
OP Multiome	10X Multiome	RNA, ATAC	Human	Bone marrow	69,249	22	13	Luecken, M et al.[2]
BMCITE	Cite-seq	RNA, ADT	Human	Bone marrow	30,672	27	1	Stuart, T. et al.[3]
OP Cite	Cite-seq	RNA, ADT	Human	Bone marrow	90,261	31	12	Luecken, M et al.[2]
Smartseq cortex	Smartseq2	RNA	Mouse	Somato sensory cortex	3005	6	1	Zeisel, A. et al.[4]
smFISH	osmFISH	RNA	Mouse	Somato sensory cortex	4530	6	1	Codeluppi, C. et al.[5]
3omics RNA	Seq-Well	RNA	Human	PBMC	16627	12	6	Wilk, A. J. et al.[6]
3omics ATAC	10X scATAC-seq	ATAC	Human	PBMC	21261	18	4	Satpathy, A. T. et al.[7]
3omics CyTOF	Helios CyTOF	Protein	Human	PBMC	43232	21	1	Covid-19 Multi-omics Blood Atlas Consortium[8]
Patch neurons	Patch-seq	RNA, morphologies	Mouse	Primary motor cortex	1214	7	1	Scala, F. et al[9]

Supplementary table 2. List of genes identified as differentially expressed in both the scRNA and scATAC gene activities for each B cell cluster.

Cluster 0	**Cluster 1**	**Cluster 2**
AIM2, BLK, CCDC50, CD1C, COTL1, CTSH, HLA-DPB1, HLA-DQA1, KCNN4, MAP4K1, MARCKS, MS4A1, OAZ1, POU2AF1, POU2F2, PPP1R15A, PTPN1, RALGPS2, SCIMP, SCRN1, SPIB, SYK, SYNGR2, TBC1D9, TFEC, TLR10, TNFRSF13B, UBC, UBE2J1, WDFY4	BCL7A, BTG1, BTLA, DGKD, FAM129C, FOXP1, HLA-DMB, ICOSLG, PCDH9, TCL1A, TSPAN13, YBX3	ACTG1, ANXA1, AOAH, APMAP, APOL3, APOL6, ARF1, ARHGEF1, ARL4C, ATP1A1, ATP2B4, ATP8B2, BCL11B, BIN2, BTN3A1, BTN3A2, BTN3A3, C11orf21, C1orf21, CAB39, CALM1, CALR, CAMK4, CANX, CBLB, CCDC88C, CCL5, CCND2, CCND3, CCSER2, CD2, CD247, CD300A, CD3D, CD3E, CD48, CD5, CD6, CD63, CD8A, CD96, CDC42SE2, CEP78, CFL1, CFLAR, CHD3, CST7, CTBP2, CTSW, CX3CR1, CYLD, CYTH1, CYTIP, DGKA, DGKZ, DIAPH1, DIP2A, DOK2, DYNC1H1, DYRK2, EFHD2, EIF3A, ESYT2, EVL, F2R, FBXW5, FCGR3A, FGD3, FGFBP2, FKBP5, FLNA, FOSL2, FYN, GBP5, GIMAP1, GIMAP4, GIMAP5, GIMAP7, GLG1, GNLY, GUK1, GZMA, GZMB, GZMH, HELZ, HERC1, HIPK1, HLA-A, HLA-B, HLA-C, HLA-E, HLA-F, HSPA5, HSPA8, ID2, IFITM1, IFITM2, IGF2R, IL10RA, IL2RB, IL32, IL6ST, IL7R, INPP4A, IQGAP2, ITGA6, ITGAL, ITGB1, ITGB2, ITK, ITM2B, JADE2, KCNAB2, KDM3A, KIAA1551, KLF13, KLRB1, KLRD1, KLRF1, KPNB1, LASP1, LCK, LCP1, LCP2, LDHB, LEF1, LINC00861, LITAF, LPIN2, MAN1A1, MATK, MBP, MCL1, MGAT4A, MLLT6, MSN, MYBL1, MYH9, MYL12A, MYL12B, MYL6, MYO1F, NCAM1, NDFIP1, NKG7, PAG1, PARP8, PBXIP1, PCED1B-AS1, PDE3B, PDZD4, PFN1, PIK3IP1, PIK3R1, PIM1, PIP4K2A, PPP2R5C, PREX1, PRF1, PRKCQ, PRMT2, PRPF38B, PRSS23, PTPN12, PTPRA, RAB27A, RAP1B, RARRES3, RASA3, RASAL3, RASGRP1, RASSF1, RASSF5, RBL2, RBMS1, REST, RICTOR, RNF125, RNF213, RPS6KA3, RUNX3, S100A4, S100A6, S1PR5, SAMD3, SAMD9, SELPLG, SEMA4D, SH2D1A, SIGIRR, SKP1, SLAMF7, SLC9A3R1, SLFN5, SMARCA2, SORL1, SPN, SPOCK2, SPTAN1, SRGN, SSBP3, ST3GAL1, STAT1, STK10, STK38, SYNE1, SYNE2, SYTL2, TAX1BP1, TBX21, TCF7, TES, TESPA1, TMC8, TNFAIP3, TNFRSF1B, TNIK, TPP2, TPST2, TRABD2A, TRAF3IP3, TRANK1, TSHZ1, TXK, UBE2G2, UTRN, VIM, WDR82, WIPF1, ZAP70, ZFP36L2, ZNF91

Supplementary table 3. List of genes identified as differentially expressed in both the scRNA and scATAC gene activities for each monocyte cluster.

Cluster 4	**Cluster 5**
ACTN1, ADAM15, ADAM8, AGTRAP, AHNAK, AHR, ALDH2, ANXA1, ANXA6, APLP2, APOL3, APP, ARHGAP26, ARHGEF40, ASGR2, ATP6V0B, ATP6V1A, ATP6V1F, BAZ2B, BHLHE40, BLVRB, BST1, CAPG, CASP4, CCDC149, CCDC88A, CCR1, CCR2, CD14, CD163, CD1D, CD63, CD84, CD93, CDA, CIITA, CKAP4, CLEC4A, CLEC4E, CLMN, CMIP, CMTM3, COMT, CPD, CPM, CREG1, CRISPLD2, CRTAP, CSF3R, CST3, CTSA, CTSH, CTSS, CXCR4, CXXC5, CYFIP1, CYP1B1, CYP27A1, DGKD, DHRS4, DYSF, EFHD2, EIF4G3, EMB, F13A1, F5, FAM129A, FAM198B, FCN1, FERMT3, FES, FKBP5, FLOT1, FNDC3B, FPR1, FRMD4B, G0S2, GAPDH, GLRX, GLT1D1, GM2A, GPX1, GRN, H2AFY, HEBP2, HEXB, HK2, HLA-A, HLA-DQB1, HLA-DRA, HLA-DRB5, HPSE, HSD17B4, IDH1, IGF2R, IGSF6, IL13RA1, IL4R, IL6R, IL6ST, IMPA2, IQGAP2, IRF2BP2, IRS2, ITGA5, ITGAM, ITGB2, IVNS1ABP, KCTD20, KDM4B, KDM7A, KIAA0040, KIF13A, KLF10, LAMP2, LAMTOR1, LAPTM5, LAT2, LBR, LGALS2, LGALS3, LINC00963, LITAF, LPGAT1, LRP1, LTB4R, LTBR, LY86, LYZ, MAPK14, MARC1, MARCO, METTL9, MGST1, MID1IP1, MLKL, MLXIP, MNDA, MPEG1, MSRB1, MYCL, MYO1F, NCF4, NFE2, NFKBIA, NLRP12, NLRP3, NR4A2, NRGN, OSCAR, P4HB, PADI2, PADI4, PARP8, PEA15, PER1, PID1, PKM, PLA2G7, PLBD1, PLD3, PLEKHO1, PLXND1, PPIF, PRRC2B, PSTPIP1, PTPRE, PYGL, QPCT, QSOX1, RAB11FIP1, RAB27A, RAB3D, RBM47, RBP7, RIT1, RPS16, RPS8, S100A10, S100A12, S100A6, S100A8, S100A9, S1PR3, SCPEP1, SEMA4D, SEPT2, SGK1, SIRPA, SLC2A3, SLC40A1, SMARCD3, SOCS3, SORL1, STAB1, STX3, SULF2, SYK, TAGLN2, TALDO1, TAPBP, TBC1D9, TET3, THBS1, TLR4, TMEM173, TMEM205, TMEM71, TNFAIP2, TNFAIP3, TNFRSF1A, TPP1, TPT1, TREM1, TRIB1, TRPS1, TSPO, TXN, VEGFA, VIM, WLS, XRN2, YBX3, YWHAE, ZNF385A, ZNF467	ACOT9, ALDH3B1, ARRDC2, ASAH1, C15orf39, CDKN1B, CDKN1C, CKB, CRIP1, CSF1R, CSK, CYTH1, FAM110A, FAM49A, FCGR3A, FOXO1, FZD1, GNAI2, GPI, GPR137B, HES4, HLA-E, HSBP1, HSPA8, IFITM2, IQSEC1, KLF11, KLF12, KLF2, KLF7, KNDC1, LFNG, LRMP, LRRC25, LRRFIP1, LYL1, LYN, MAFB, MEG3, METRNL, MGLL, MRPS35, MS4A7, MTSS1, MYO1G, MYOF, NECAP2, PDPK1, PIK3CG, PILRA, PKN1, PPP1R17, PSAP, PTP4A2, PTPN1, PTPRC, RALB, RHOB, RIN3, RNH1, RRAS, SAT1, SFT2D2, SLC44A2, SMAD2, SNX5, SPG11, SPRED1, SSBP4, TPTEP1, UNC119, VPS35, WARS, WAS, XIAP, YBX1, ZBTB7A, ZFAND5, ZFR, ZNF703

Supplementary Table 4. Results of the differential expression analysis for the cluster 6 of monocytes in the tri-omics experiment. The output of scanpy's rank_gene_groups method (which uses a one versus all two-sided t-test with benjamini-hochberg correction) is displayed for two known marker genes of monocyte-derived dendritic cells.

names	**scores**	**logfoldchanges**	**pvals**	**pvals_adj**
CCR7	2.67e+01	5.40e+00	2.06e-157	9.74e-154
CD2	2.15e+01	5.61e+00	2.75e-102	8.79e-100

Supplementary Table 5. List of the number of features measured in each modality of the datasets used and the number of neurons in hidden layers of the autoencoders .

Dataset Name	**Number of features**	**Hidden size**
Cell lines/RNA	>10000	64
Cell lines/ATAC	>10000	64
PBMC 10X/RNA	>10000	64
PBMC 10X/ATAC	>10000	64
OP Multiome/RNA	>10000	64
OP Multiome/ATAC	>10000	64
BMCITE/RNA	>10000	64
BMCITE/ADT	25	20
OP Cite/RNA	>10000	64
OP Cite/ADT	134	32
Smartseq cortex	>10000	64
smFISH	33	25
Covid RNA	>10000	64
Hemato ATAC	>10000	64
Covid CyTOF	48	32
Neurons/RNA	>10000	64
Neurons/Images	2048	128

Supplementary table 6. Comparison of the running times of the benchmarked methods on the 10X PBMC dataset (9,378 cells per modality).

Method	Device	Runtime
Seurat_v3	CPU	12mn 18s
LIGER	CPU	5mn 49s
MultiMAP	CPU	2mn 6s
Uniport	GPU	56mn 59s
scGLUE	GPU	32mn 24s
scConfluence	GPU	23mn 38s

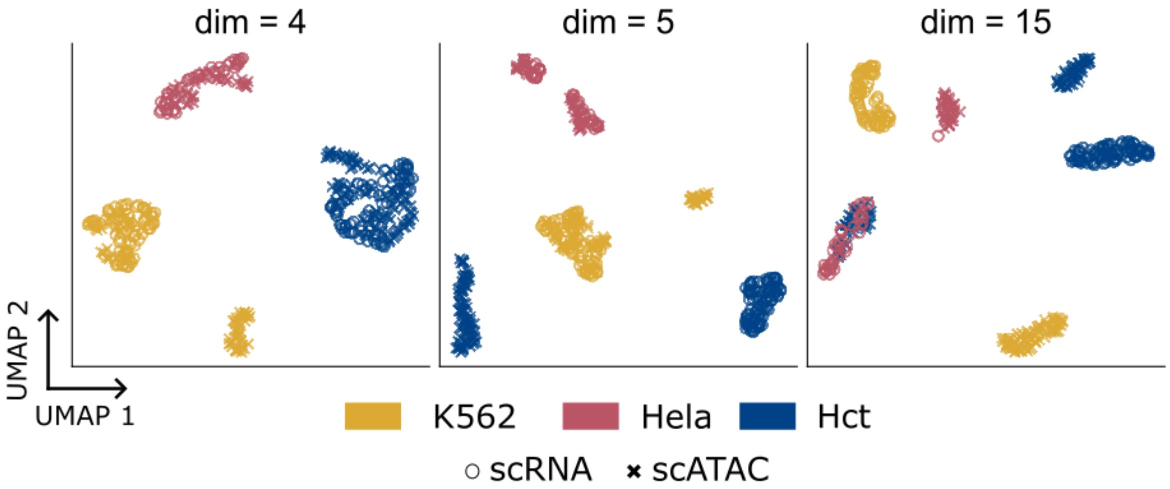

Supplementary Figure 1. 2D UMAP visualizations of the cell embeddings obtained by LIGER on the cell lines dataset for different values of the dimension of the latent space. Different colors in these UMAP plots correspond to the three different cell lines present in the data while the shape of the point markers correspond to the modality of origin of each cell (scRNA, scATAC).

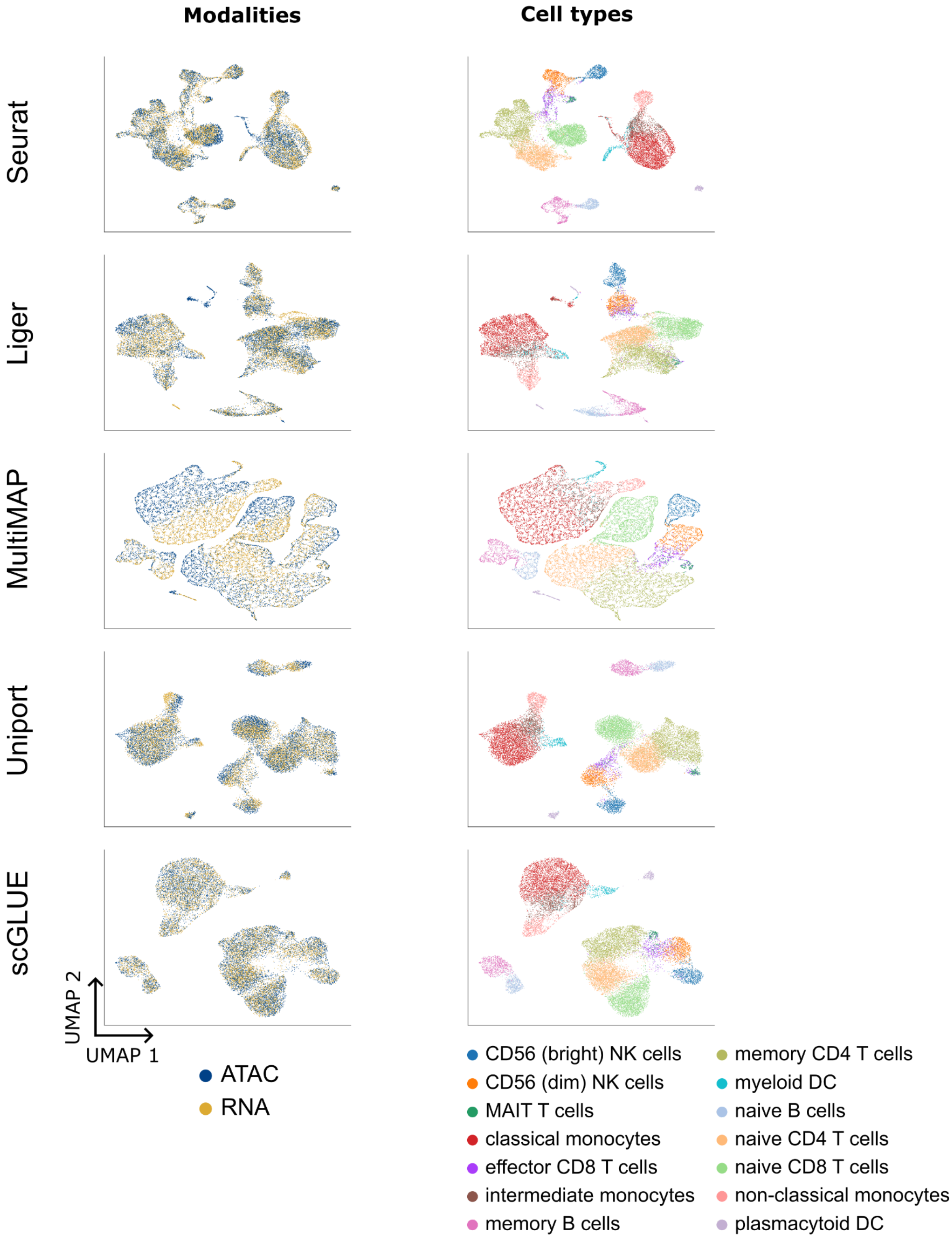

Supplementary Figure 2. 2D UMAP visualizations of the cell embeddings obtained by the five baselines (Seurat, Liger, MultiMAP, Uniport and scGLUE) on the *PBMC 10X* dataset. Cells are colored based on their modality of origin and their cell type annotation.

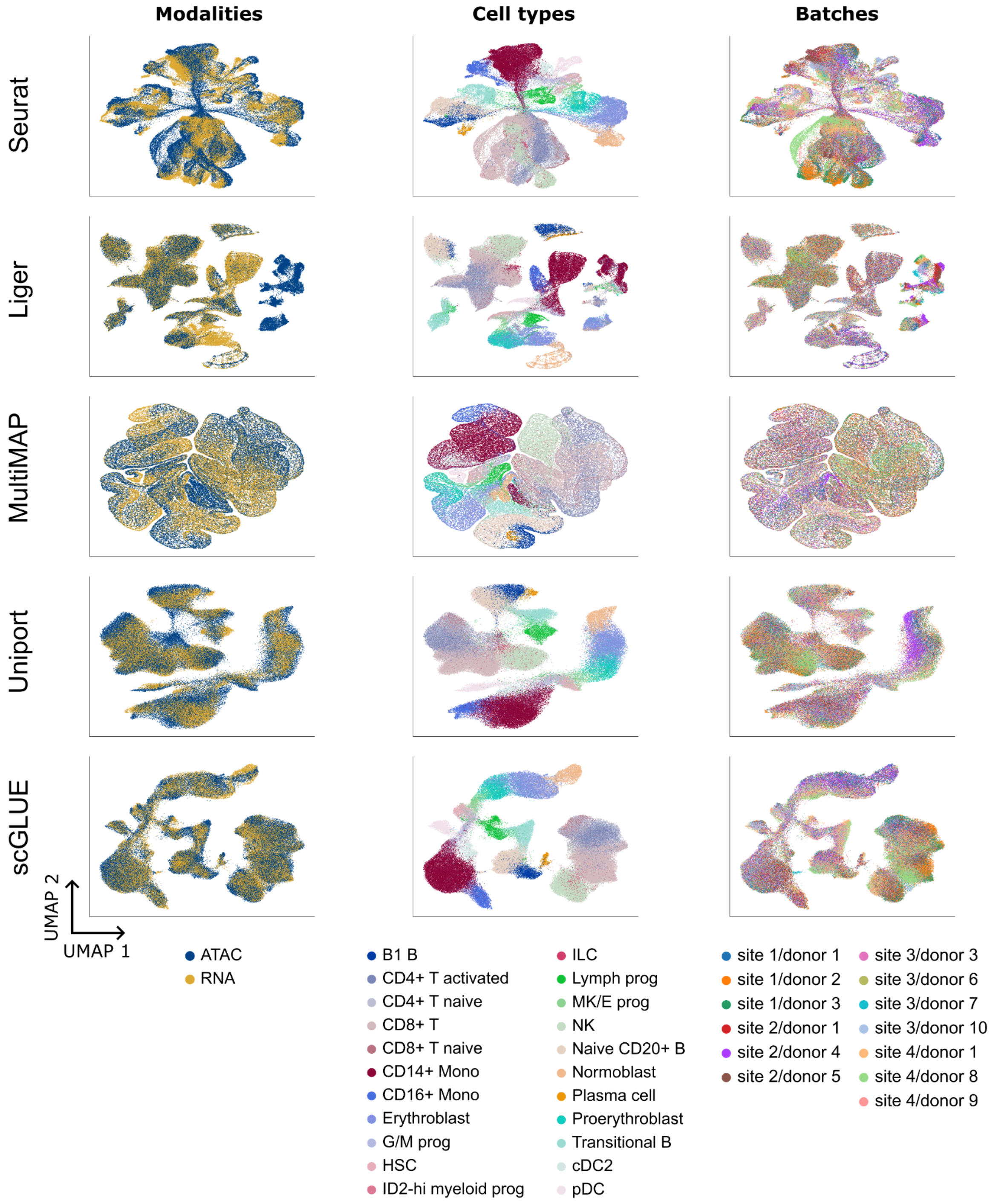

Supplementary Figure 3. 2D UMAP visualizations of the cell embeddings obtained by the five baselines (Seurat, Liger, MultiMAP, Uniport and scGLUE) on the *OP Multiome* dataset. Cells are colored based on their modality of origin, their cell type annotation or their batch of origin.

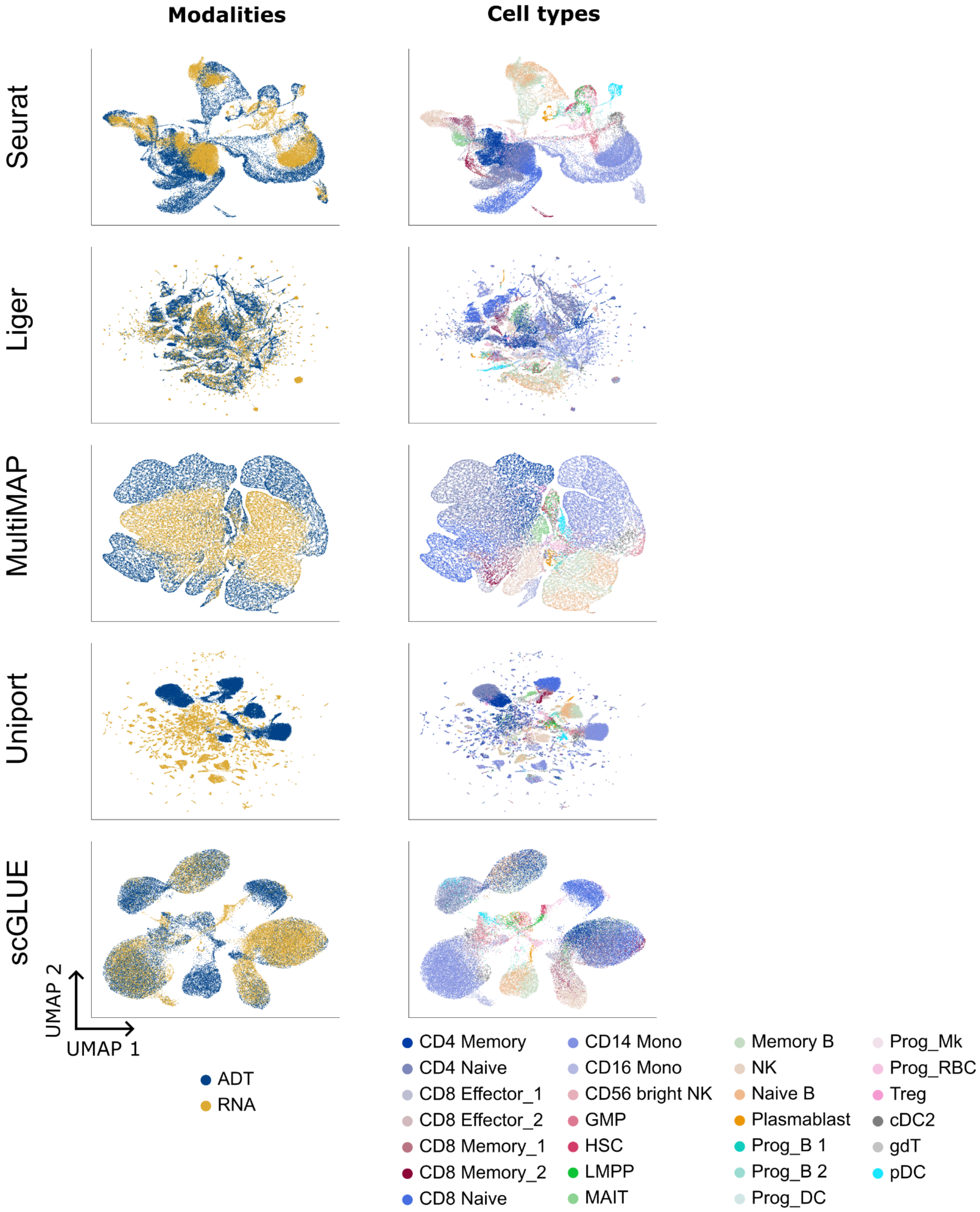

Supplementary Figure 4. 2D UMAP visualizations of the cell embeddings obtained by the five baselines (Seurat, Liger, MultiMAP, Uniport and scGLUE) on the *BMCITE* dataset. Cells are colored based on their modality of origin or their cell type annotation.

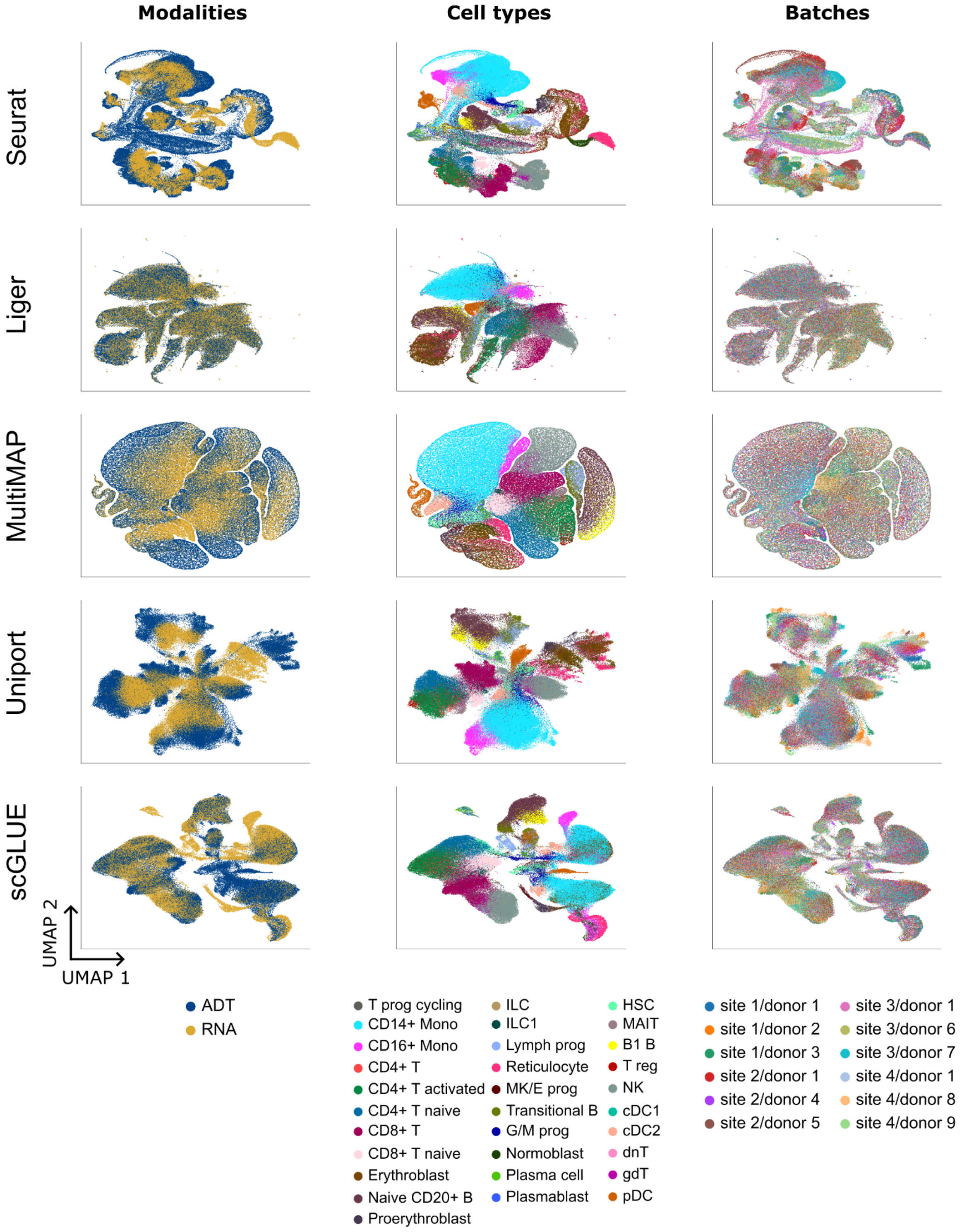

Supplementary Figure 5. 2D UMAP visualizations of the cell embeddings obtained by the five baselines (Seurat, Liger, MultiMAP, Uniport and scGLUE) on the *OP Cite* dataset. Cells are colored based on their modality of origin, their cell type annotation or their batch of origin.

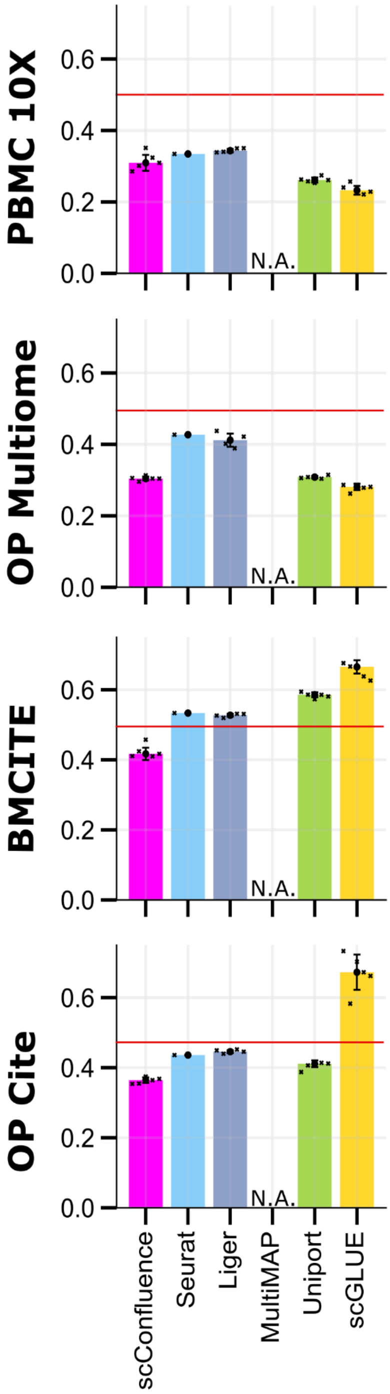

Supplementary Figure 6. Evaluation of the cell type FOSCTTM for all methods on the four benchmark datasets as well as the cell lines dataset. The horizontal line y=0.5 is the theoretical result of the trivial approach which consists in the random alignment of cells from the same cell type across modalities. Error bars in the plots specify the standard deviation across n=5 random initialization seeds for each method and they are centered on the median result. Inside bar plots, small dark stars represent individual seed results. Source data are provided as a Source Data file.

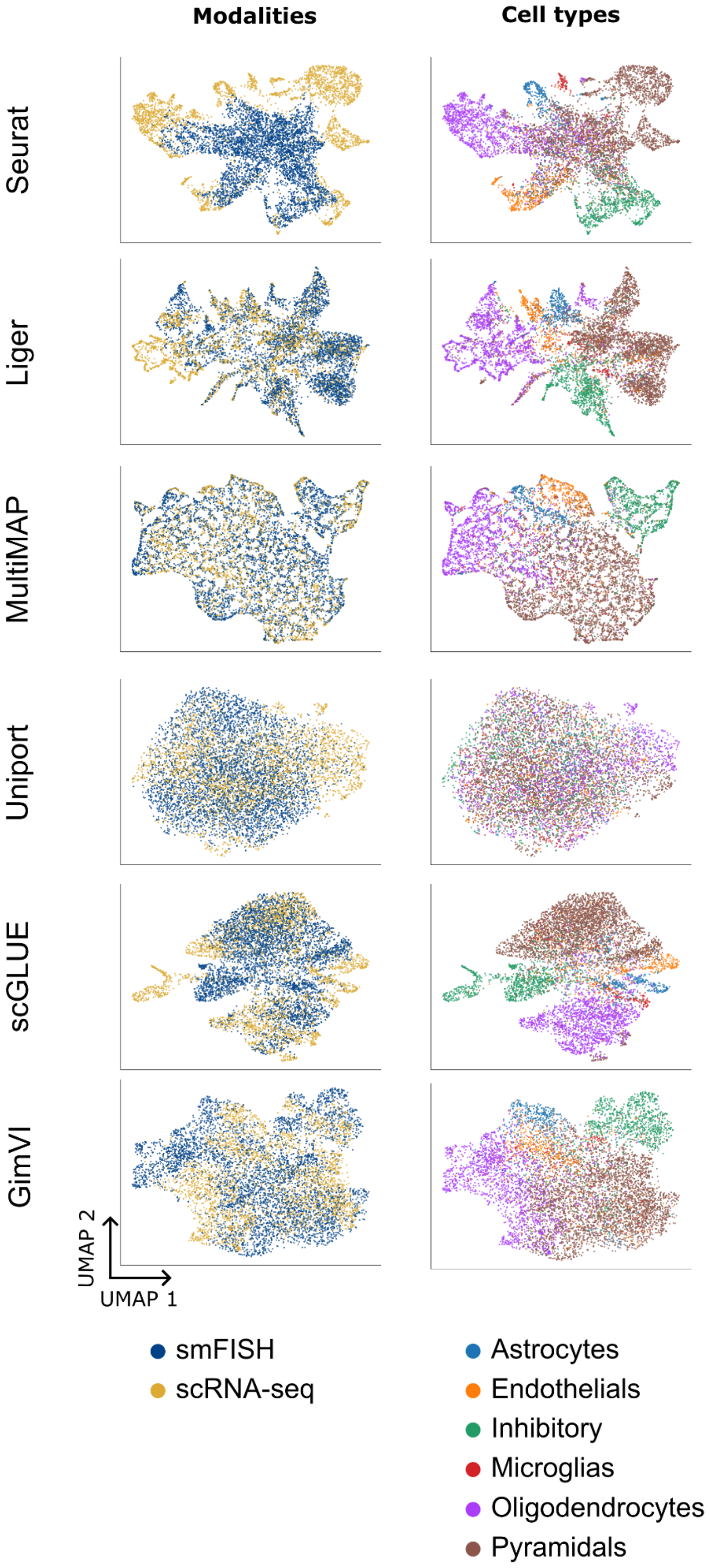

Supplementary Figure 7. 2D UMAP visualizations of the cell embeddings obtained by the six baselines (Seurat, Liger, MultiMAP, Uniport, scGLUE and GimVI) on the *scRNA/smFISH* dataset. Cells are colored based on their modality of origin and their cell type annotation.

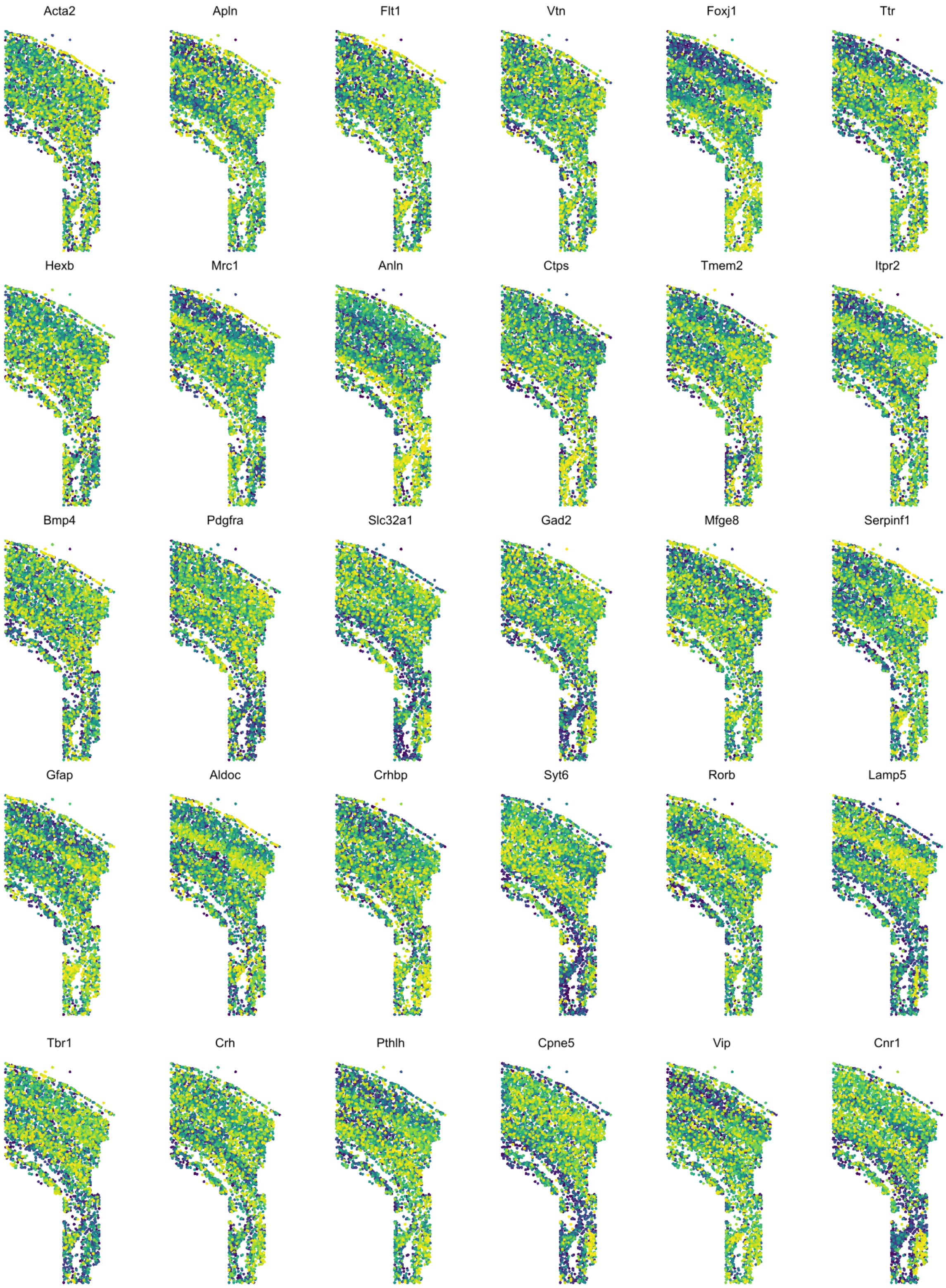

Supplementary Figure 8. Spatial pattern of expression of scConfluence's imputations on the thirty held-out smFISH genes which were not displayed in Figure 6.

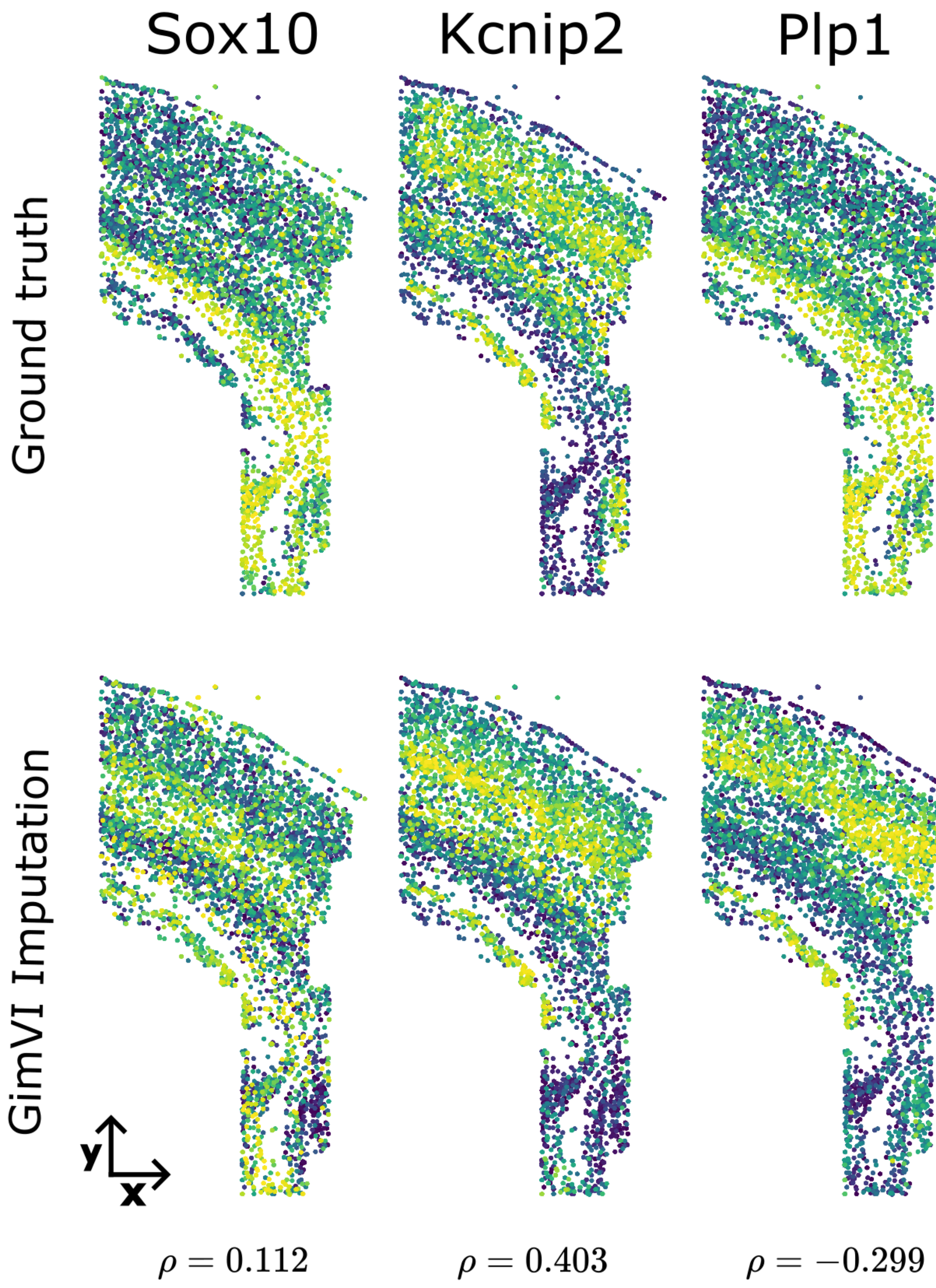

Supplementary Figure 9. Spatial pattern of expression of GimVI's imputations (bottom) on three held-out smFISH genes and their ground-truth pattern of expression (top). Spearman correlations between the ground-truth and imputed counts are written at the bottom.

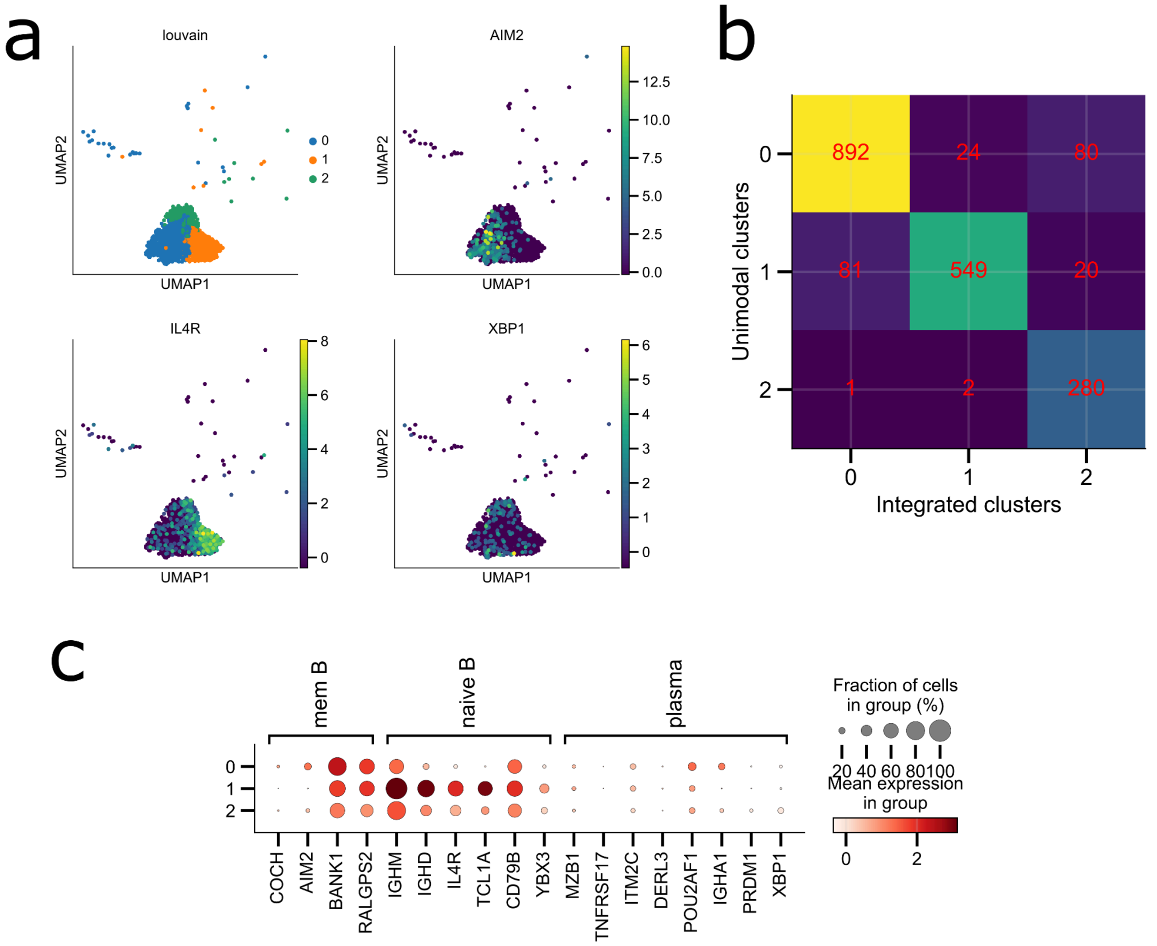

Supplementary Figure 10. Heterogeneity inside the scRNA B cells. (a) scRNA B cell clusters derived from a unimodal analysis and marker expressions. (b) Comparison of the cluster obtained in the tri-omics integration analysis and clusters obtained by analyzing the scRNA B cells on their own. (c) Dotplot of known marker genes of memory, naive and plasma B cells.

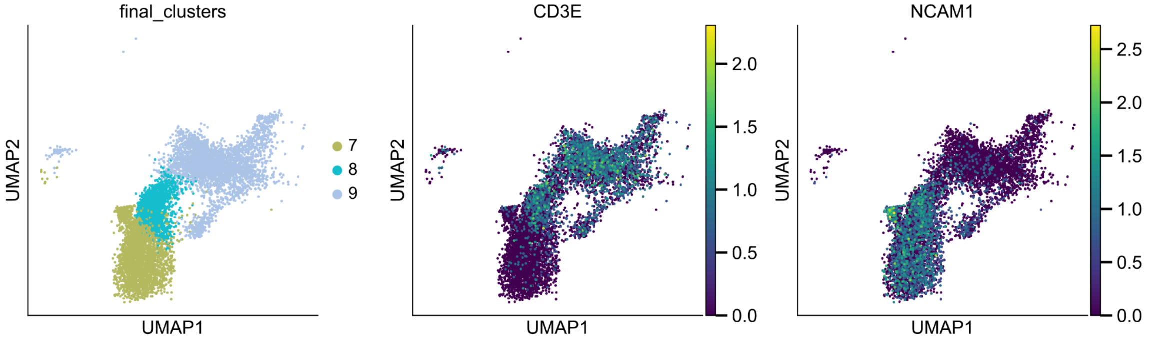

Supplementary Figure 11. scRNA NKT cells. UMAP 2D projections of scConfluence's cell embeddings of scRNA cells in cluster 7, 8 and 9. Cells are colored based by their cluster annotation and their level of expression of CD3E and NCAM1 which are markers of CD8 T cells and NK cells respectively.

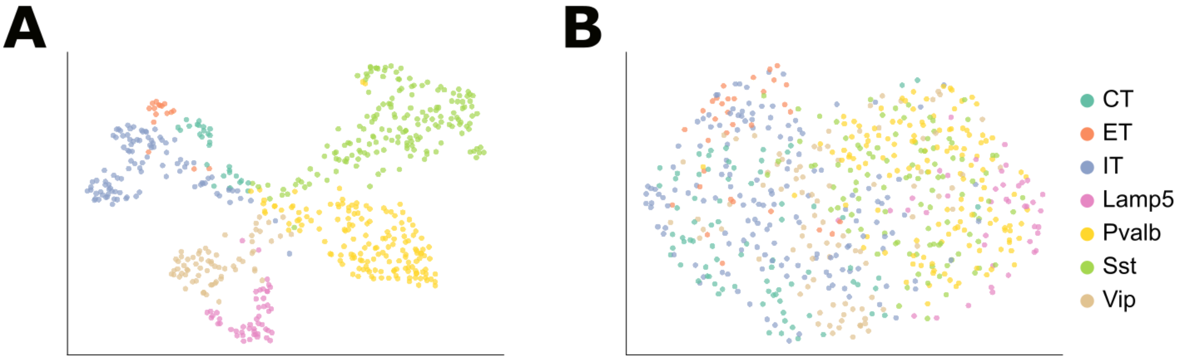

Supplementary Figure 12. Unimodal embeddings of scRNA-seq and morphologies before integration. UMAP visualizations of cell embeddings obtained by training independent autoencoders on the two modalities, (a) scRNA counts and (b) neuronal morphologies, without integrating them together. Cell embeddings are colored by their transcriptomic cell type annotations.

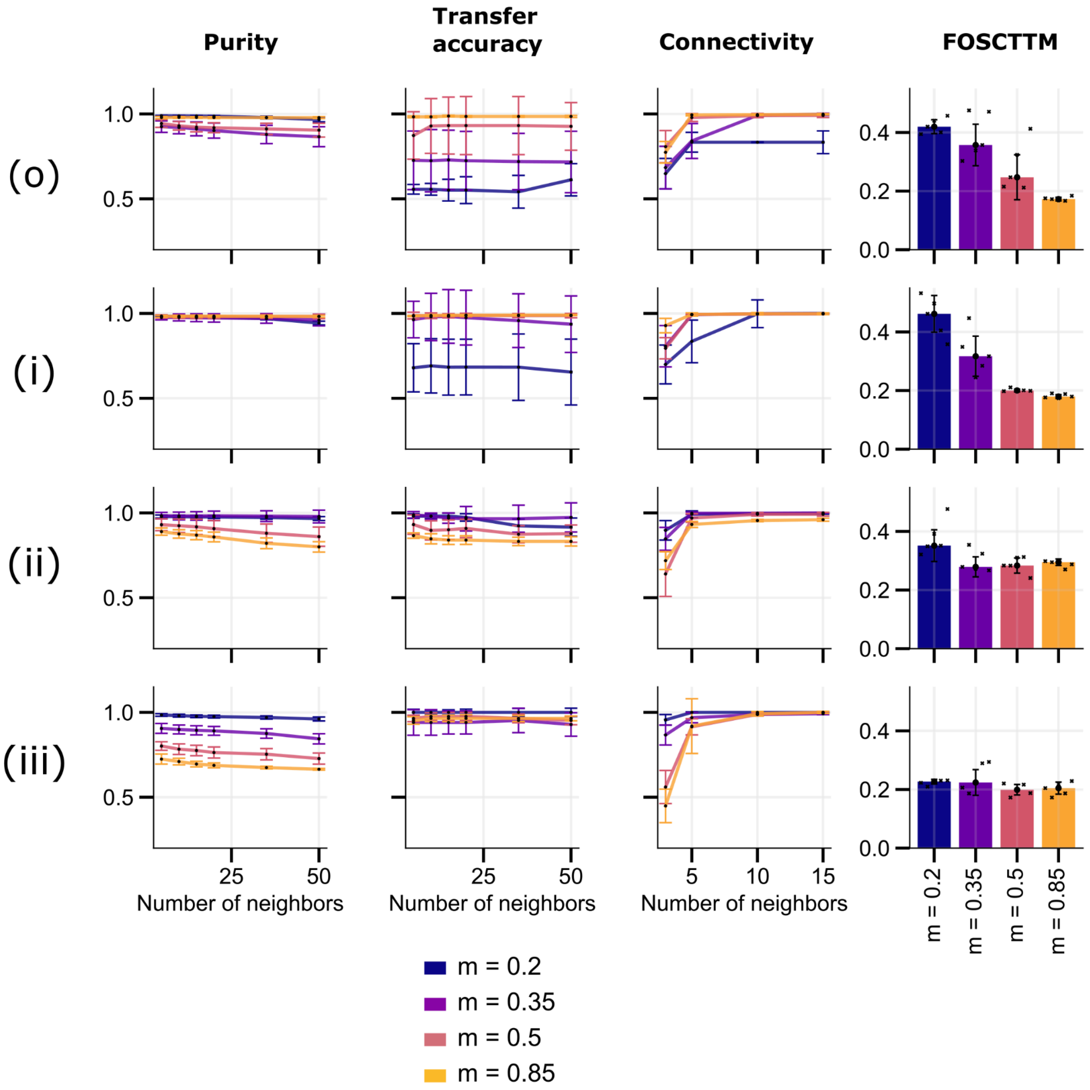

Supplementary Figure 13. The impact of the mass parameter for different degrees of unbalancedness. Using the same evaluation metrics and datasets as in Figure 2, we compare the results of training of the scConfluence model with different values of the mass parameter m. Error bars in the plots specify the standard deviation across n=5 random initialization seeds for each method and they are centered on the median result. Inside bar plots, small dark stars represent individual seed results. Source data are provided as a Source Data file.

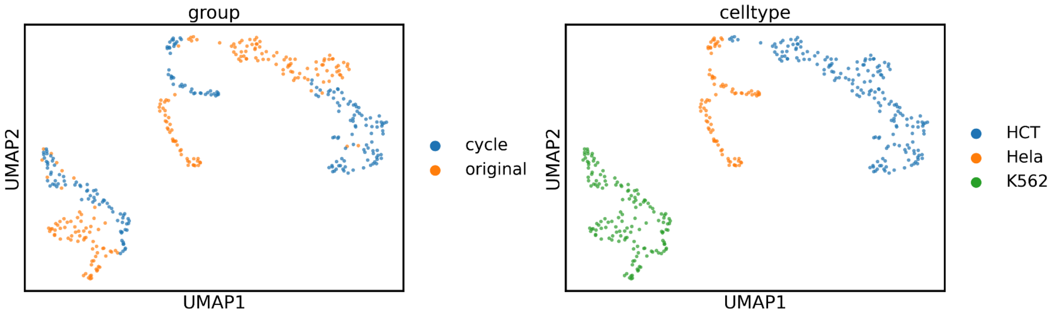

Supplementary Figure 14. 2D UMAP visualizations of the scRNA cell embeddings obtained by scConfluence. The “original” embeddings correspond to scRNA cells directly encoded to the latent space while the “cycle” embeddings are results of applying first the ATAC modality’s decoder then the ATAC modality’s encoder to the “original” embeddings.

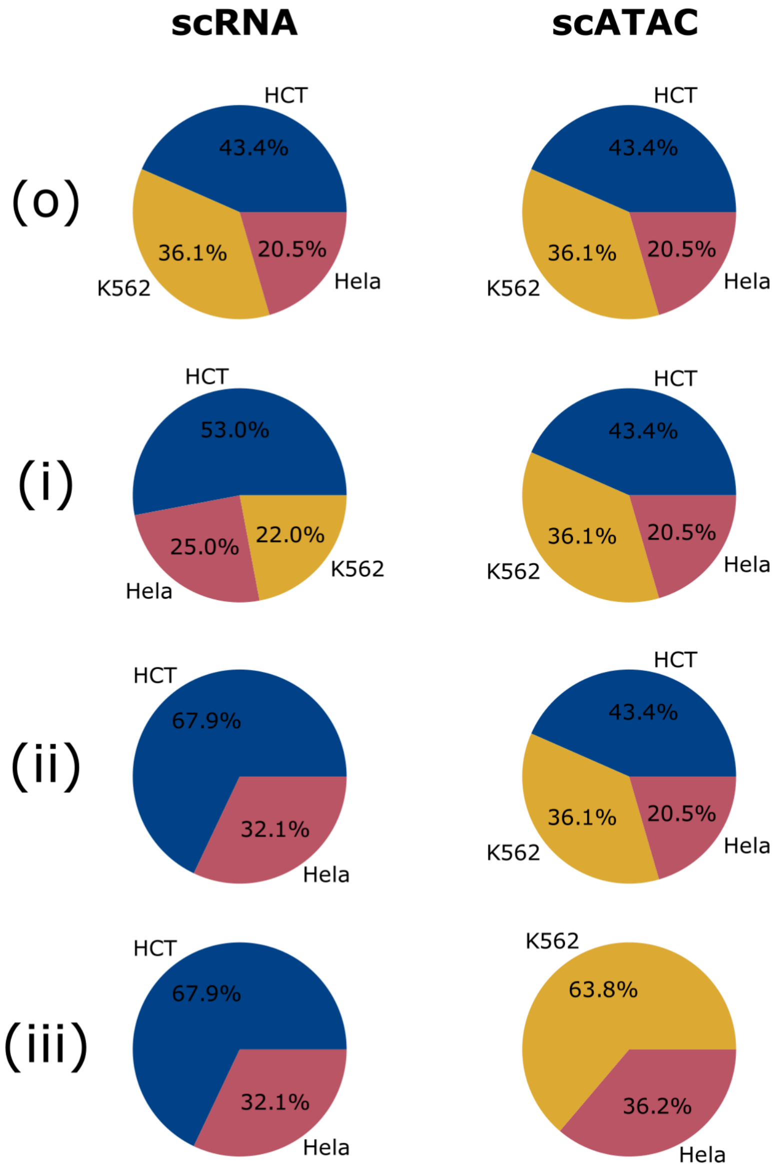

Supplementary Figure 15. Proportions of cell types present in each modality across the four cell lines scenarios in the first experiment. Source data are provided as a Source Data file.

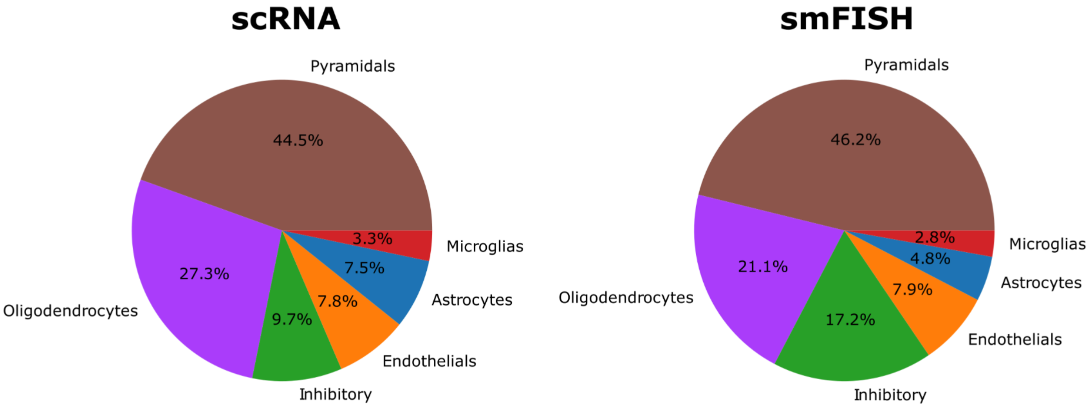

Supplementary Figure 16. Proportions of cell types present in each modality of the mouse somatosensory cortex experiment. Source data are provided as a Source Data file.

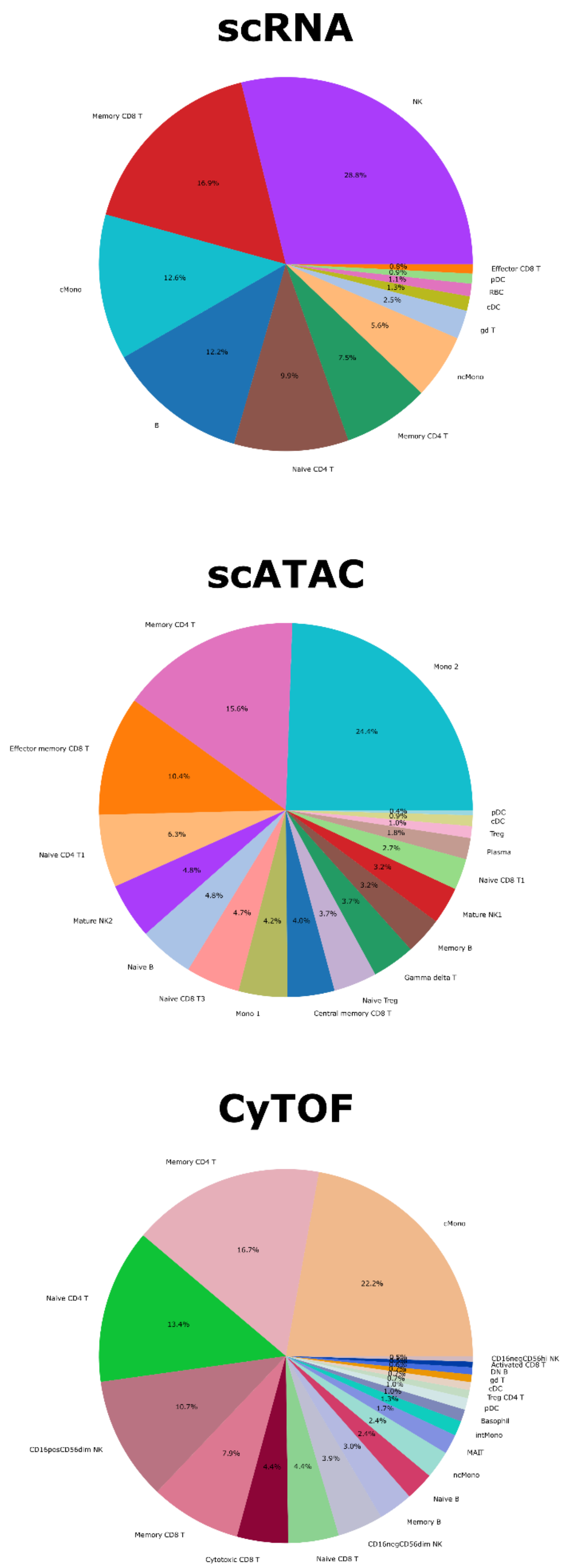

Supplementary Figure 17. Proportions of cell types present in each modality of the tri-omics PBMC experiment. Source data are provided as a Source Data file.

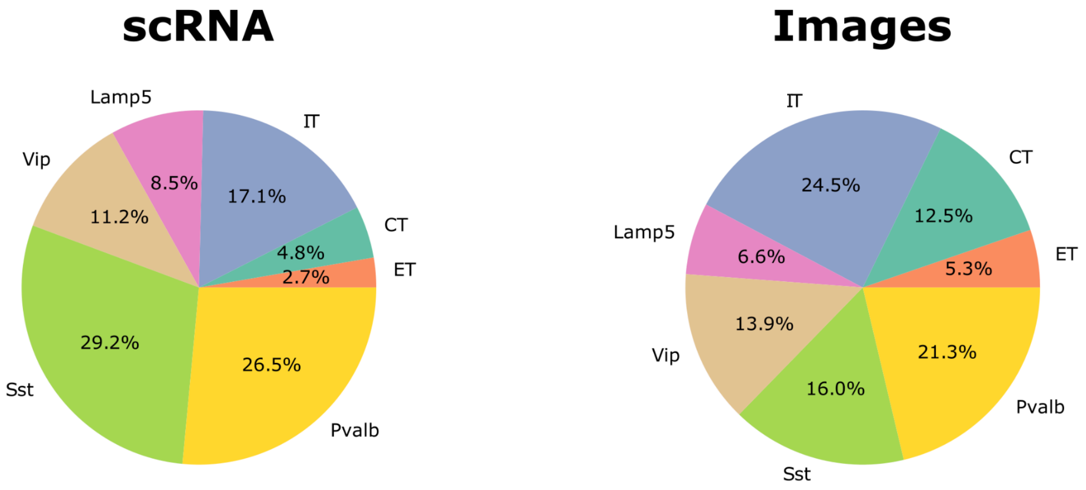

Supplementary Figure 18. Proportions of cell types present in each modality of the Patch-seq experiment. Source data are provided as a Source Data file.